Title

elPBN neurons regulate rVLM activity through elPBN-rVLM projections during activation of cardiac sympathetic afferent nerves.

Journal

American journal of physiology. Regulatory, integrative and comparative physiology, 311(2)

ISSN

0363-6119

Authors

Guo, Zhi-Ling
Longhurst, John C
Tjen-A-Looi, Stephanie C
et al.

Publication Date

2016-08-01

DOI

10.1152/ajpregu.00127.2016

Peer reviewed

Am J Physiol Regul Integr Comp Physiol 311: R410–R425, 2016.
First published May 25, 2016; doi:10.1152/ajpregu.00127.2016.

elPBN neurons regulate rVLM activity through elPBN-rVLM projections during activation of cardiac sympathetic afferent nerves

Zhi-Ling Guo, John C. Longhurst, Stephanie C. Tjen-A-Looi, and Liang-Wu Fu

Department of Medicine and Susan-Samueli Center for Integrative Medicine, School of Medicine, University of California at Irvine, Irvine, California

Submitted 31 March 2016; accepted in final form 16 May 2016

Guo ZL, Longhurst JC, Tjen-A-Looi SC, Fu LW. elPBN neurons regulate rVLM activity through elPBN-rVLM projections during activation of cardiac sympathetic afferent nerves. *Am J Physiol Regul Integr Comp Physiol* 311: R410–R425, 2016. First published May 25, 2016; doi:10.1152/ajpregu.00127.2016.—The external lateral parabrachial nucleus (elPBN) within the pons and rostral ventrolateral medulla (rVLM) contributes to central processing of excitatory cardiovascular reflexes during stimulation of cardiac sympathetic afferent nerves (CSAN). However, the importance of elPBN cardiovascular neurons in regulation of rVLM activity during CSAN activation remains unclear. We hypothesized that CSAN stimulation excites the elPBN cardiovascular neurons and, in turn, increases rVLM activity through elPBN-rVLM projections. Compared with controls, in rats subjected to microinjection of retrograde tracer into the rVLM, the numbers of elPBN neurons double-labeled with c-Fos (an immediate early gene) and the tracer were increased after CSAN stimulation ($P < 0.05$). The majority of these elPBN neurons contain vesicular glutamate transporter 3. In cats, epicardial bradykinin and electrical stimulation of CSAN increased the activity of elPBN cardiovascular neurons, which was attenuated ($n = 6$, $P < 0.05$) after blockade of glutamate receptors with iontophoresis of kynurenic acid (Kyn, 25 mM). In separate cats, microinjection of Kyn (1.25 nmol/50 nl) into the elPBN reduced rVLM activity evoked by both bradykinin and electrical stimulation ($n = 5$, $P < 0.05$). Excitation of the elPBN with microinjection of DL-homocysteic acid (2 nmol/50 nl) significantly increased basal and CSAN-evoked rVLM activity. However, the enhanced rVLM activity induced by DL-homocysteic acid injected into the elPBN was reversed following iontophoresis of Kyn into the rVLM ($n = 7$, $P < 0.05$). These data suggest that cardiac sympathetic afferent stimulation activates cardiovascular neurons in the elPBN and rVLM sequentially through a monosynaptic (glutamatergic) excitatory elPBN-rVLM pathway.

glutamate; neuronal activity; brain stem; heart; cardiovascular responses

ACTIVATION OF CARDIAC SYMPATHETIC afferent nerves, especially during myocardial ischemia, causes cardiac pain and excitatory reflex cardiovascular responses characterized by increases in sympathetic outflow, elevations in blood pressure (BP) and heart rate (HR), and tachyarrhythmia (11, 12, 24, 34). These reflex responses increase the morbidity and mortality of patients with heart diseases, because they exacerbate the extent of ischemia and infarction, which leads to severe heart failure and lethal ventricular arrhythmias (11, 24, 34). We have demonstrated that a number of metabolites produced during myocardial ischemia, including bradykinin (BK) and adenosine 5′-triphosphate (ATP), among others, activate cardiac sympathetic afferent nerves (CSAN) and evoke sympathoexcitatory reflex responses (11, 12, 24). However, how the central nervous system processes inputs from CSAN and, ultimately, regulates reflex cardiovascular responses is largely unknown.

Brain stem regions, such as the rostral ventrolateral medulla (rVLM) and nucleus of the solitary tract (NTS), are crucial in the regulation of cardiovascular function (1, 3, 7, 18, 22, 30). We and others have identified a population of neurons that fire in synchrony with the cardiac cycle and are sensitive to baroreceptor activation in both nuclei (1–3, 18, 22). These cells are classified as cardiovascular neurons (1–3, 18, 22). Cardiovascular neurons in the rVLM and NTS are involved in central processing of reflex cardiovascular responses (3, 7, 8, 18). Other studies have suggested that the lateral division of the parabrachial nucleus (LPBN), including the external lateral subdivision (elPBN), contains a heterogeneous population of neurons involved in regulation of both respiratory and cardiovascular function (13, 23, 29). Some LPBN neurons have been reported to mediate respiratory changes accompanying changes in BP (23, 35). We have observed that cardiac sympathetic afferent stimulation activates neurons in the elPBN (16, 17) and evokes pressor reflexes that are reduced after inhibition of the elPBN (11), suggesting that the cardiovascular neurons responsive to cardiac afferent input likely also exist in the elPBN. Thus the present study was designed to determine if cardiovascular neurons are present in the elPBN and to examine their contribution to central processing of cardiac sympathetic afferent input.

There are connections between PBN subnuclei and other brain stem autonomic centers, including a connection between the elPBN and the VLM (7, 13). The rVLM, specifically, is an important brain region that critically controls sympathetic outflow and cardiovascular function. Anatomical evidence shows direct connections between the elPBN and the rVLM, although their functional neurotransmitter system has not been identified (35). Physiological studies in rats have shown that chemical stimulation of the LPBN, including the elPBN, with glutamate increases activity of the rVLM neurons (1, 28), implying the existence of an excitatory connection between these two nuclei. Although we have shown anatomically that elPBN neurons are activated by cardiac sympathetic afferent inputs (16, 17), whether these neurons project directly to the rVLM and facilitate activation of rVLM cardiovascular neurons through glutamate is not known.

Therefore, we hypothesized that cardiac sympathetic afferent stimulation excites elPBN cardiovascular neurons and, in turn, rVLM cardiovascular neurons through direct glutamatergic elPBN-rVLM connections. Using anatomical and electrophysiological approaches, in the present study we sought to identify elPBN cardiovascular neurons that are activated by cardiac sympathetic afferent stimulation and directly project to

Address for reprint requests and other correspondence: Z.-L. Guo, Dept. of Medicine, C240 Medical Science 1, Univ. of California, Irvine, Irvine, CA 92697-4075 (e-mail: zguo@uci.edu).

the rVLM. Thus the present study investigated the influence of elPBN neurons on the activity of rVLM cardiovascular neurons through excitatory elPBN-rVLM projections associated with glutamate during cardiac sympathetic afferent stimulation.

METHODS

All procedures in animals were carried out in accordance with the guidelines of the American Physiological Society and the National Institutes of Health. The minimum possible number of animals was used to obtain reproducible and statistically significant results. In addition, every effort was made to minimize discomfort and suffering. Surgical and experimental protocols were approved by the Animal Care and Use Committee at the University of California at Irvine. Previous studies have shown that rats and cats display similar cardiovascular and autonomic responses to cardiac afferent nerve stimulation. The central neural anatomy and circuits associated with processing cardiac inputs are virtually identical in the rat and the cat (6, 7, 21, 25, 42, 49). The advantage of cats is their size, which facilitates placement of multiple or closely spaced recording and stimulating electrodes. Rats were used in tract-tracing studies requiring survival for 7–10 days.

Anatomical Experiments

Microinjection of retrograde tracer into the rVLM. Adult male Sprague-Dawley rats (350–500 g body wt) were used for microinjection of a retrogradely transported microsphere tracer into the rVLM to visualize direct projections from the elPBN to the rVLM, as described in our previous studies (31, 36). Briefly, a mixture of ketamine and xylazine (80 and 12 mg/ml, respectively; Sigma Chemical, St. Louis, MO) was used to induce (0.3–0.4 ml im) and maintain (0.1–0.2 ml im) anesthesia in the animals. Body temperature was monitored with a rectal probe and maintained at 37°C. HR and O_2 saturation were monitored using a pulse oximeter (Nonin Medical, Plymouth, MN). After induction of anesthesia, rats were positioned in a stereotaxic apparatus (David Kopf Instruments). A 1-inch incision was made to expose the skull. A burr hole (4 mm diameter) was made in the bone unilaterally, so that a glass micropipette could be inserted using the following coordinates: 12.0–12.5 mm caudal from bregma, 2.0–2.5 mm lateral from midline, and 8.5 mm below the dural surface (31, 37). Microinjection of DL-homocysteic acid (DLH, 2 nmol/50 nl) was used to tentatively identify the location of the rVLM, noted as an increase in HR. We then injected a retrogradely transported tracer (50 nl), rhodamine-labeled fluorescent microspheres in suspension (0.04 μm; Molecular Probes, Eugene, OR), into the rVLM through a glass micropipette (20- to 30-μm tip diameter). After being taken up avidly by presynaptic terminals (26, 44), the fluorescent microspheres filled the cell soma. These fluorescent microspheres are not toxic to the neuron, are easily recognized, and remain very stable for years. Thus they are considered reliable retrograde tracers for examination of neuronal pathways (44, 46). After microinjection of the microsphere retrograde tracer, the wound was sutured shut.

Terminal procedures were carried out 7–10 days after administration of the retrograde tracer. Rats were reanesthetized with ketamine-xylazine as described above. An adequate depth of anesthesia, as judged by stability of respiration, BP, and HR and lack of a withdrawal response to toe pinch, was maintained. A femoral artery and vein were cannulated for measurement of arterial BP (model P 23 ID, Statham, Oxnard, CA) and administration of drugs and fluids, respectively. HR was derived from the arterial pressure pulse with a biotach (Gould Instrument, Cleveland, OH). The animal was ventilated artificially through a cuffed endotracheal tube after intubation. Arterial blood gases and pH were monitored with a blood gas analyzer (model ABL-3, Radiometer, Westlake, OH) and kept within normal limits (P_{O_2} 100–150 mmHg, P_{CO_2} 28–35 mmHg, pH 7.35–7.45) by adjustment of the volume and/or the ventilation rate, enrichment of the inspired O_2 supply, and administration of 1 M $NaHCO_3$. Body temperature was maintained at 36–37.5°C by a water heating pad and a heat lamp. Bilateral cervical vagotomy and barodenervation with sectioning of carotid sinus nerves were performed to eliminate parasympathetic, as well as potentially baroreflex, inputs to the elPBN during cardiac sympathetic afferent activation (16, 17). Successful barodenervation was evaluated by the absence of reflex bradycardia (decreases in HR by 21–25 vs. 0–3 beats/min, barointact vs. barodenervated) when BP was increased [increases in mean arterial blood pressure (MAP) by 23–27 vs. 18–24 mmHg, barointact vs. barodenervated] following bolus injections of phenylephrine (1 μg/100 g iv).

Experimental protocols. Rats subjected to microinjection of the retrograde tracer into the rVLM were divided randomly into cardiac sympathetic afferent stimulation and control groups. Similar to our previous studies (16, 17), a small incision was made between the left third and sixth ribs after removal of the fourth and fifth ribs to expose the anterior surface of the heart. A pledget (0.6 cm^2) of filter paper soaked with a solution of α,β-methylene-ATP (α,β-meATP) or 0.9% normal saline was placed on the epicardial surface of the myocardium. In the cardiac sympathetic afferent-stimulated group, 40-μl doses of α,β-meATP (0.2–0.6 mg/ml, leading to increases in BP) were applied every 20 min for a total of six applications over a 100-min period (10). In control animals, 0.9% normal saline, the vehicle for α,β-meATP, was applied repeatedly.

Immunohistochemical staining. TISSUE PREPARATION. As described in our previous studies (31, 36), at 90 min after termination of cardiac sympathetic afferent or control stimulation, deep anesthesia was induced by another larger dose of ketamine-xylazine (0.5–0.7 ml im). Transcardial perfusion was performed using 500 ml of 0.9% saline solution followed by 500 ml of 4% paraformaldehyde in 0.1 M phosphate buffer (pH 7.4). The pons and medulla oblongata were removed and treated with 4% paraformaldehyde and 30% sucrose. Coronal sections (30 μm) were cut on a cryostat microtome (model CM1850, Leica, Nussloch, Germany) to identify sites of microsphere tracer injection and to perform immunohistochemical labeling, as described below. Free-floating sections were used for labeling.

C-FOS IMMUNOHISTOCHEMICAL LABELING. Sections were stained for c-Fos to identify elPBN cells activated by cardiac sympathetic nerve stimulation (16, 17). After they were washed for 30 min (3 times for 10 min each) in phosphate-buffered saline containing 0.3% Triton X-100 (PBST, pH 7.4), brain sections were placed for 1 h in 1% normal donkey serum (Jackson ImmunoResearch Laboratories, West Grove, PA). The sections were incubated with a primary polyclonal rabbit anti-Fos antibody (1:2,000 dilution; Oncogene Research Products, Calbiochem, San Diego, CA) at 4°C for 48 h. After they were rinsed three times in PBST, the tissues were incubated with a fluorescein-conjugated donkey anti-rabbit antibody (1:200 dilution; Jackson ImmunoResearch Laboratories) for 24 h at 4°C. Each section was mounted on a slide and air-dried. Coverslips were mounted on the slides using VECTASHIELD mounting medium for fluorescence (catalog no. H-1000, Vector Laboratories, Burlingame, CA). In immunohistochemical control studies, all c-Fos staining was abolished when 1 ml of the diluted primary antibody was preincubated with 5 μg of the immunizing peptide corresponding to amino acids 4–17 of human c-Fos (SGFNADYEASSSRC; catalog no. PP10, Oncogene Research Products, Calbiochem). In addition, no labeling was detected when the primary or secondary antibody was omitted.

DOUBLE-FLUORESCENT IMMUNOHISTOCHEMICAL LABELING FOR C-FOS + VESICULAR GLUTAMATE TRANSPORTER 3. Vesicular glutamate transporter (VGLUT) specifically transports glutamate into vesicles of neurons and, thus, offers a unique marker to distinctively identify neurons that use glutamate as a neurotransmitter (9, 15, 17, 32). While VGLUT1 and VGLUT2 antisera mainly label nerve fibers, VGLUT3 antiserum shows the staining pattern of both cell bodies and nerve fibers (17, 32). We and others have shown that VGLUT3-containing neurons are located in the PBN and are responsive to

peripheral nerve stimulation (17, 48). To determine if c-Fos nuclei were colocalized with the perikarya of rVLM-projecting glutamatergic neurons following stimulation of cardiac sympathetic afferents, we selected VGLUT3 as the marker for glutamatergic neurons in the present study. The staining procedures were similar to those used for single-fluorescent immunohistochemical labeling described above. Briefly, after treatment with PBST and 1% normal donkey serum, brain tissues were incubated with two primary antibodies: a rabbit polyclonal anti-c-Fos antibody (1:2,000 dilution) and a guinea pig anti-VGLUT3 antibody (1:500 dilution; catalog no. AB5421, Chemicon, Temecula, CA) that was used to stain for cell bodies in the rat (32) for 48 h at 4°C. Sections then were incubated with a coumarin-conjugated donkey anti-rabbit antibody and a fluorescein-conjugated donkey anti-guinea pig antibody (all 1:100 dilution; Jackson ImmunoResearch Laboratories) at 4°C for 24 h. The sections were mounted on slides, and mounting medium (Vector Laboratories) was used to apply coverslips. In the immunohistochemical control studies, no stain was detected when the primary or secondary antibody was omitted. In addition, the specificity of the VGLUT3 antibody was verified further by preabsorption with an excess amount (10 μg/ml) of VGLUT3 peptide (Chemicon).

DATA ANALYSIS. Brain sections were scanned and examined with a standard fluorescence microscope (model E400, Nikon, Melville, NY) that was equipped with three epifluorescence filters (B-2A, G-2A, or UV-2A) to detect green, red, and blue colors. Sections containing the elPBN were identified according to their best-matched standard stereotaxic plane, as shown in the atlas of Paxinos and Watson for the rat (37). Two sections were selected for each of two representative planes (bregma −9.00 and −9.24 mm; Fig. 2) of the pons that contain elPBN in all animals.

Selected sections were further evaluated with a laser scanning confocal microscope (LSM 510, Meta System, Zeiss, Thornwood, NY) to confirm colocalization of two or three labels. This apparatus was equipped with argon and HeNe lasers and allowed operation of multiple channels. Lasers of 488- and 543-nm wavelengths were used to excite fluorescein (green) and rhodamine (red), respectively. A 790-nm laser was applied for two-photon excitation of coumarin (blue). Digital fluorescent images were captured and analyzed with software (Zeiss LSM) provided with the confocal microscope. Each confocal section analyzed was limited to 0.5-μm thickness in the z plane. Images containing two or three colors in the same plane were merged to reveal the relationship between two or three labels (Fig. 1). In each animal, the number of single-, double-, and/or triple-labeled cells was counted. The proportion of the double-labeled neurons relative to single-labeled neurons was calculated as a percentage. The average of these values, derived from the two representative planes (Fig. 2), was used to represent the average value of these data per section for statistical analysis (16, 17).

Physiological Experiments

Animal preparations. GENERAL SURGICAL PREPARATION. Studies were performed in cats (2.9–4.6 kg body wt) of either sex. The animals were preanesthetized with ketamine (20–30 mg/kg im) and anesthetized with α-chloralose (40–50 mg/kg iv) through the femoral vein. Additional α-chloralose (5–10 mg/kg iv) was given as needed to maintain an adequate depth of anesthesia, assessed by observing the absence of a conjunctival reflex. The trachea was intubated with a cuffed endotracheal tube, and respiration was maintained artificially (model 661, Harvard ventilator, Ealing, South Natick, MA). Arterial blood gases and body temperature were maintained within physiological limits as described above in the rat subjected to terminal surgical procedures. To vagotomize the animals, parasympathetic branches of vagus nerves to the heart and lungs were cut bilaterally ~1 cm above the aortic arch.

CARDIAC SYMPATHETIC NERVE STIMULATION. We have described chemical and electrical cardiac sympathetic nerve stimulations in detail in our previous studies (18, 41). Briefly, to chemically stimulate CSAN, a small incision was made through the left fourth or fifth intercostal space to expose the pericardium. A PE-60 catheter with six perforations in its distal end was introduced into the pericardium for intrapericardial application of BK and 0.9% normal saline. To electrically stimulate CSAN, the left inferior cardiac branch of the sympathetic nerve was isolated through a sternotomy approach. A bipolar flexible platinum stimulating electrode was placed around the intact nerve branch. The stimulating electrode was connected to an isolation unit and stimulator (model S88, Grass Instruments) to deliver bipolar stimuli. Slight increases in BP (5–10 mmHg) and HR (~10 beats/min) following electrical stimulation (2 Hz and 0.5-ms pulses at 1–4 mA) confirmed correct isolation of cardiac sympathetic nerves (41). CSAN-induced activity in the elPBN and rVLM was obtained with a lower intensity (~0.4 mA) of stimulation that did not cause changes in BP and HR. The stimulating electrode was held in place with epoxy dental glue (Pentron, Wallington, CT). After these procedures, the ribs were approximated and the chest was closed.

RENAL SYMPATHETIC NERVE ACTIVITY. To correlate renal sympathetic nerve activity (RSNA) with rVLM discharge activity, multiunit RSNA was recorded as described previously (18, 31, 36). Briefly, under a dissecting microscope, a branch of the renal nerve from surrounding connective tissue was isolated and cut distally to eliminate afferent discharge. The nerve was covered with warm mineral oil and placed across one pole of a bipolar recording electrode that was attached to a high-impedance probe. The other pole of the recording electrode was grounded with a normal saline-presoaked cotton thread to the animal. The signals were amplified and processed through an audio amplifier with the low-frequency cutoff set at 30 Hz and the high-frequency cutoff set at 3 kHz. The amplified signals were processed and recorded with a computer through an analog-to-digital converter for subsequent off-line analysis. Discharge activity of the renal sympathetic nerve was analyzed with data acquisition-and-analysis software (Spike 2, Cambridge Electronic Design). Electrical noise level in neural recordings was determined after the nerves were crushed at the end of the experiment.

ACCESSING BRAIN NUCLEI. Animals were placed in a stereotaxic head frame (Kopf Instruments). A craniotomy was performed to expose the dorsal surface of the brain stem for unilateral microinjection, stimulation, and recording of extracellular activity in the same side of the elPBN and rVLM (11, 31, 36). To access the elPBN, we performed a unilateral cerebellectomy to visualize the surface of the pons. A single- or multi-barrel glass micropipette was positioned 9.5–11 mm rostral to obex, 5.0–5.4 mm lateral to midline at a 90° angle to the dorsal surface of the pons at a depth of 0.8–1.8 mm to reach the elPBN (4, 11, 16, 17, 35). To access the rVLM, the glass micropipette was positioned 2.9–3.5 mm rostral to obex and 3.0–3.6 mm lateral to midline at a 90° angle to the dorsal surface of the medulla at a depth of 5.0 mm (36, 42). The glass micropipette was positioned by a micromanipulator (Kopf). The locations of the elPBN and rVLM were identified preliminarily by the pressor and tachycardia responses during chemical (e.g., DLH) stimulation and confirmed histologically after the experiment.

MICROINJECTION AND IONTOPHORESIS IN BRAIN NUCLEI. Unilateral microinjection (50 nl) of a chemical was performed using a glass micropipette (15- to 20-μm tip diameter) that was connected to a microsyringe injector (model UMP3) and contained a 10-μl Hamilton syringe (WPI, Sarasota, FL) (11). To record and iontophorese a chemical into the same neuron, we used a triple-barrel glass pipette electrode (~3-μm maximum total tip diameter) to record neuronal activity and to iontophorese the chemical in the area of interest (18, 42). One barrel of the pipette electrode was filled with the chemical. Another barrel contained a platinum recording electrode with 0.5 M sodium acetate containing 2% Chicago sky blue (Sigma Chemical). The third barrel was filled with 3 M sodium chloride to balance the current in the iontophoresis system (Neurophore BH2 system, Med-

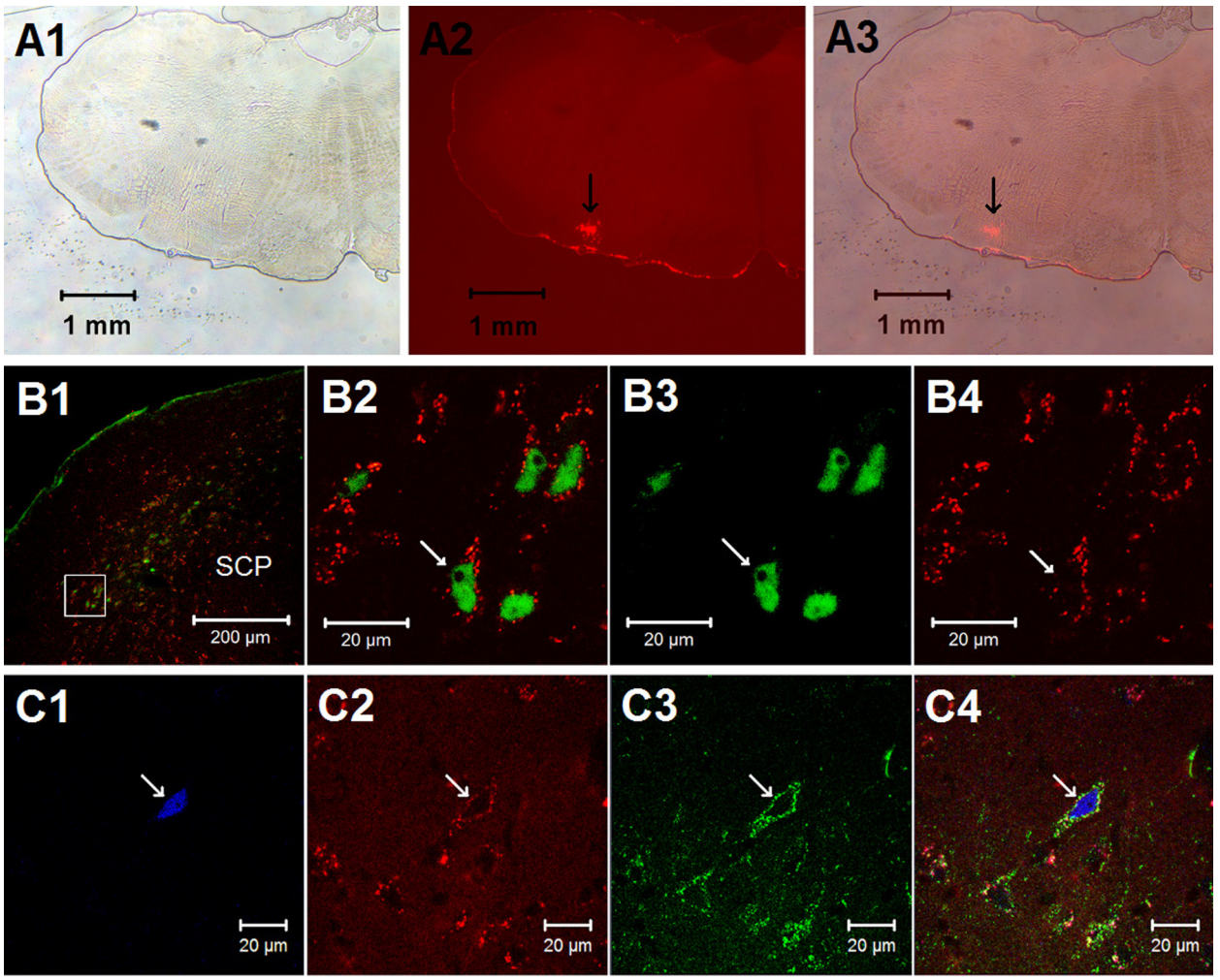

Fig. 1. Histological staining in the external lateral parabrachial nucleus (elPBN) and the rostral ventrolateral medulla (rVLM). *A1–A3*: photomicrographs demonstrating a microinjection site of the retrograde microsphere tracer in the rVLM [bregma −12.12 mm; from the rat brain atlas of Paxinos and Watson (37)]. *A1*: bright-field image of a medulla section. *A2*: fluorescence image showing the microinjection site of the retrograde microsphere tracer in the medulla section. *A3*: merged image from *A1* and *A2*. Arrows in *A2* and *A3* indicate the injection site located in the rVLM. *B* and *C*: confocal microscopic images showing double (*B1–B4*) and triple (*C1–C4*) fluorescent labeling in the elPBN (bregma −9.00 mm) of a rat following stimulation of cardiac sympathetic afferent nerves with epicardial application of α,β-methylene-ATP (α,β-meATP, 8 μg). *B1*: low-power photomicrograph. *B2*: higher magnification of the region within the box (located in the elPBN) in *B1*. *B2* is a merged image from *B3* and *B4*. Arrows in *B2*, *B3*, and *B4* indicate a neuron labeled with c-Fos + tracer, c-Fos (green), and tracer (red), respectively. SCP, superior cerebellar peduncle. Arrows in *C1, C2, C3,* and *C4* indicate a neuron containing c-Fos (blue), retrogradely transported microspheres originating from the rVLM (red), vesicular glutamate transporter 3 (green), and colocalization of the 3 labels.

ical Systems, Greenvale, NY). The retention current for balancing was +25 to −10 nA. The chemical was injected over a 2-min period with 10- to 120-nA currents, depending on the structure of the injected chemical.

SINGLE-UNIT EXTRACELLULAR RECORDING AND IDENTIFICATION OF A CARDIOVASCULAR NEURON. A glass micropipette containing a platinum electrode was advanced ventrally in 1- to 2-μm steps toward the elPBN or rVLM to detect spontaneous neuronal activity or activity evoked by electrical CSAN stimulation (2 Hz). The neuronal activity was amplified with a preamplifier (model P511, Grass Instruments) attached to a high-impedance probe (model H1P5, Grass Instruments) and then filtered (0.3–10 kHz) and monitored with an oscilloscope (Tektronix 2201). The neuronal signals then were transferred to a computer for analysis (Spike 2). Care was taken to minimize the influence of respiratory and BP change-related movements on the recorded neuronal activity by application of a bilateral pneumothorax and administration of gallamine triethiodide (4 mg/kg iv) every 2 h. Spike discrimination was closely monitored throughout the experiment. To characterize a cardiovascular neuron, its barosensitivity was tested by recording changes in discharge rate in response to a decrease and/or an increase in BP elicited by administration of nitroglycerin (50 μg/kg iv) and/or phenylephrine (2.5 μg/kg iv), respectively. For further characterization, spontaneous activity was recorded for 300 s. The presence of rhythmicity related to the cardiac cycle (i.e., cardiac rhythmicity) in the spontaneous neuronal activity was determined by evaluation of pulse synchronization with frequency and time domain analyses. After identification of the neuron, analysis of peristimulus histograms was used to examine evoked responses to electrical CSAN stimulation (30 stimuli at 2 Hz) and BK was used to examine responses to epicardial stimulation. To determine sympathetic activity of the cardiovascular neuron in the rVLM, the relationship between rVLM neuronal activity and RSNA also was assessed with both time and frequency domain analyses using spike-triggered averaging and coherence analysis, as described below.

To determine direct functional projections of cardiovascular elPBN neurons to the rVLM, we identified antidromically evoked elPBN neuronal activity by stimulating the rVLM at a frequency of 2 Hz for 0.5 ms, as we and others have described previously (31,

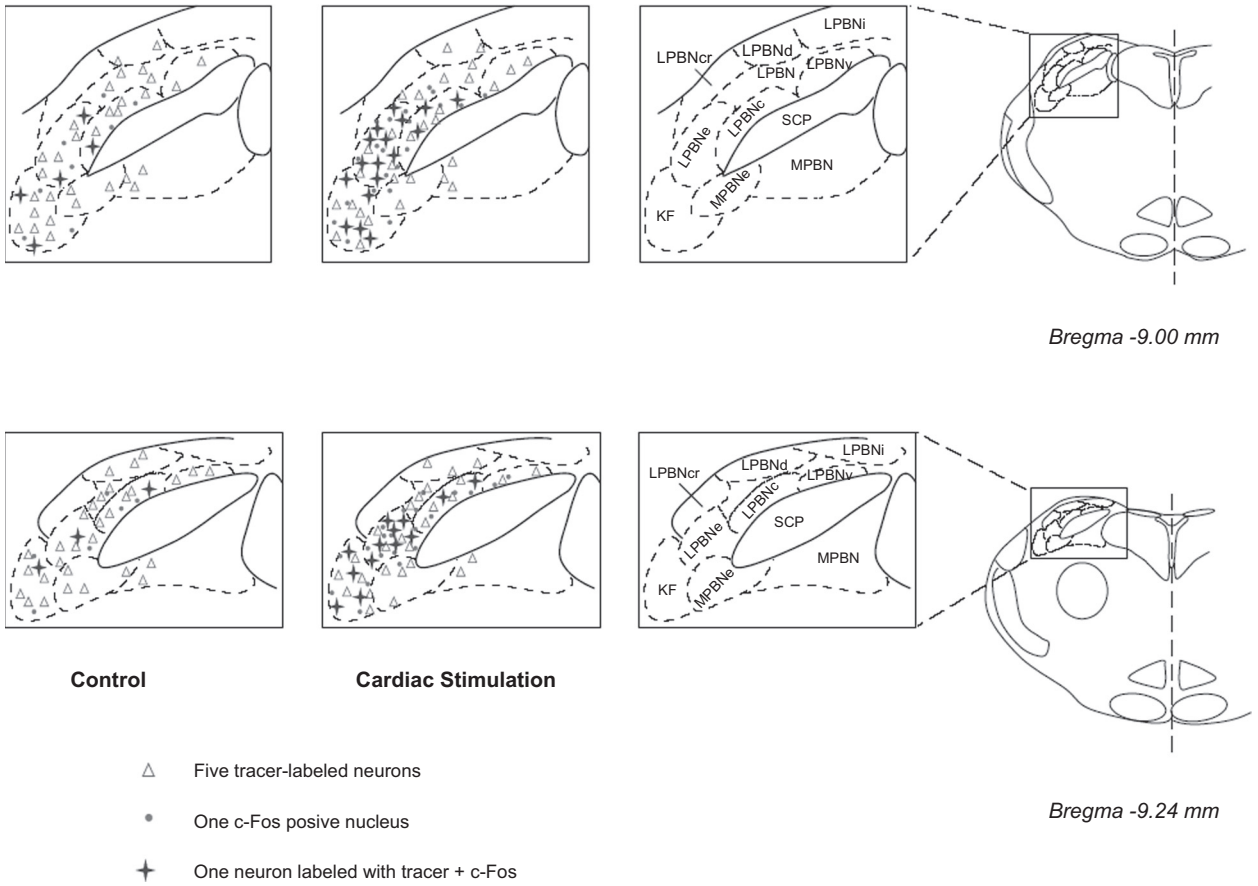

Fig. 2. Distribution of c-Fos immunoreactivity and/or cells labeled with retrograde microsphere tracer in the elPBN following epicardial stimulation with α,β-meATP (8 μg) and in a sham-operated control. Two coronal sections of the pons ipsilateral to the tracer injection in the rVLM [atlas of Paxinos and Watson (37)] were selected from 1 animal in each experimental group. Each symbol represents a labeled cell(s). SCP, superior cerebellar peduncle; PBN, parabrachial nucleus; LPBN, lateral PBN; LPBNc, central part of LPBN; LPBNcr, crescent part of LPBN; LPBNd, dorsal part of LPBN; LPBNe, external part of LPBN; LPBNi, internal part of LPBN; LPBNv, ventral part of LPBN; MPBN, medial PBN; MPBNe, external part of MPBN; KF, Kölliker-Fuse nucleus.

33, 36, 42). Briefly, elPBN neurons that responded to antidromic stimulation were examined for constant latency, stable threshold of the evoked all-or-none response, and a faithful response to high rates of stimulation (>200 Hz). Then these elPBN neurons were evaluated for collision of rVLM-evoked antidromic action potentials and orthodromic activity evoked by CSAN. The refractory period was also measured to determine the critical time interval (latency + refractory period) during which the ortho- and antidromic spikes collide. The conduction velocity of elPBN neurons was determined from the distance between the recording and stimulating electrodes and the antidromic latency.

HISTOLOGY. At the end of each experiment, the medulla and pons were removed and submerged in 10% paraformaldehyde for ≥2 days. Frozen coronal 50-μm sections were cut with a microtome cryostat (Leica). Sites of microinjection and iontophoresis were marked by spots of Chicago sky blue and identified according to the atlas of Berman (4, 11, 18, 36).

DRUGS. Kynurenic acid (Kyn, 25 mM) is a specific glutamate ionotropic receptor antagonist (11, 45); DLH (40 mM) is a specific glutamate ionotropic receptor agonist (38, 47). Each drug was dissolved in artificial cerebrospinal fluid (aCSF, pH 7.4) or 0.9% normal saline mixed with Chicago sky blue (2%) for subsequent histological site verification (18). For epicardial stimulation, we used α,β-meATP (0.2–0.6 mg/ml), a specific $P2X_1$ and $P2X_3$ receptor agonist, or BK (1–10 μg/ml); both were dissolved in 0.9% normal saline. As demonstrated in our previous studies, consistent pressor responses were observed in the rat with repeated epicardial application of α,β-meATP (10) and in the cat with BK (11, 18, 19). Thus, α,β-meATP and BK were administered to the rat and cat, respectively. All chemicals were purchased from Sigma-Aldrich, prepared weekly, and stored in a freezer at −20°C.

Experimental Protocols

Excitation of elPBN cardiovascular neurons in response to CSAN stimulation through activation of glutamate receptors. Only elPBN cardiovascular neurons were selected for study in this protocol. To identify direct elPBN-rVLM projections, in some cases, we examined the activity of elPBN cardiovascular neurons evoked by antidromic stimulation in the rVLM. To examine the responses of elPBN cardiovascular neurons to cardiac afferent stimulation, we recorded their responses to epicardial application of BK (1–10 μg/ml, 50 μl) and electrical CSAN stimulation (30 stimuli at 2 Hz). The dose of BK was based on previous studies (11, 16, 18). Finally, we measured the responses of the elPBN neuron to chemical and electrical CSAN stimulations 5 min after iontophoresis of Kyn (25 mM) with currents of 80–120 nA or 0.9% normal saline (vehicle for Kyn) into the elPBN to determine the role of the glutamate receptors in excitation of elPBN cardiovascular neurons during CSAN stimulation. This dose of Kyn in the elPBN markedly attenuates sympathoexcitatory reflex responses induced by cardiac stimulation with BK (11).

Response of the rVLM cardiovascular neuron during CSAN stimulation before and after blockade of glutamate ionotropic receptors in the elPBN or rVLM. A single-barrel micropipette was positioned into the elPBN for microinjection, and a single- or triple-barrel micropipette was positioned in the ipsilateral rVLM for recording and iontophoresis in a cat. An rVLM cardiovascular neuron was identified as described in SINGLE-UNIT EXTRACELLULAR RECORDING AND IDENTIFICATION OF A CARDIOVASCULAR NEURON. In addition, to characterize the rVLM cell with sympathetic activity, the relationship between rVLM neuronal activity and RSNA was evaluated by RSNA spike-triggered averaging and coherence analyses. After identification, we conducted the following protocols.

In *protocol 1*, we examined rVLM activity in response to CSAN stimulation before and after microinjection of Kyn into elPBN. At 20 min following identification of an rVLM cardiovascular neuron responsive to CSAN input, we microinjected Kyn (1.25 nmol/50 nl) into the ipsilateral elPBN. Then we evaluated the rVLM response to epicardial stimulation with BK (1–10 μg/ml in 50 μl) and electrical CSAN stimulation. Control animals were assessed in an identical manner with elPBN microinjection of the vehicle, aCSF.

In *protocol 2*, we evaluated the responses of rVLM neurons during DLH-induced elPBN excitation in the absence and presence of CSAN stimulation before and after iontophoresis of Kyn into the rVLM. After identification of an rVLM cardiovascular neuron responsive to chemical and electrical CSAN stimuli, we measured basal and CSAN-evoked rVLM activity before and after microinjection of DLH (2 nmol/50 nl) into the ipsilateral elPBN. The dose of DLH was shown to significantly excite neurons (38, 47). After 20 min, Kyn or vehicle (0.9% normal saline) was iontophoresed into the rVLM and the elPBN was stimulated again with DLH. We then reassessed basal and CSAN-evoked rVLM activity before and after microinjection of DLH. Since aCSF was the vehicle for DLH, microinjection of aCSF into the elPBN described in *protocol 1* also served as the control for microinjection of DLH into the elPBN in *protocol 2*.

NEUROPHYSIOLOGICAL DATA ANALYSIS. RSNA and single-unit extracellular recordings were evaluated and analyzed during and after experiments. Action potentials were assessed visually and with the Spike 2 program using wave-shape recognition algorithms to allow detection of similar wave shapes and heights. A window discriminator was set just above the noise level, so that only renal nerve discharge was counted. Nerve discharge also was rectified and averaged over a 10-s period with the software (Spike 2) to assess integrated RSNA (11, 18).

The activity of the elPBN or rVLM neurons in response to chemical stimulation with BK or to baroreceptor loading/unloading is presented as the average of the total number of spikes over time [impulses (imp)/s]. Peristimulus time histogram analysis was used to quantitatively assess elPBN and rVLM neuronal responses during brief electrical CSAN stimulation (30 stimuli over 15 s), as described previously (31, 42). As shown in Fig. 7, the analysis occurred over 0.5 s, beginning 0.1 s before and lasting 0.1–0.4 s after electrical CSAN stimulation. Evoked activity by CSAN stimulation during the 30 stimuli was calculated as the sum of spikes during 0.1 s of the peak response poststimulation minus spikes over a similar time period recorded immediately before stimulation. Thus it indicated the total evoked discharge induced by 30 CSAN stimuli over and above baseline.

COHERENCE ASSESSMENT. Frequency domain analysis was used to assess coherence of elPBN or rVLM neuronal activity with arterial BP or RSNA using a fast Fourier transform algorithm (18, 27, 31, 42). We recorded data using a sampling rate of 10,000 Hz (see Fig. 3). The original data were reconstructed by averaging every 10 points to a single point that provided a new sampling rate of new data series of 1,000 Hz. In the resampled data series, BP was generated from the mean of 10 coterminous original values. The value of the neural activity was obtained from the mean, maximum, and minimum data from the slope and amplitude of the original spike to preserve action potentials. The spikes were sorted and identified with a window discriminator to construct histograms. The number of data sections (15–20, each lasting 12.8 s) was chosen to determine the average histogram. Thus coherence was generated with seven overlapping windows, each with a duration of 12.8 s, consisting of 256 bins with 50-ms bin widths. The autospectral analysis was adopted from Shin et al. (40) using contiguous segments of 256 beats with 50% overlap between the segments. The frequency resolution was 1/12 s or 0.08 Hz. The coherence function (normalized cross-spectrum) provided a measure of the strength of the linear correlation of two signals at each frequency (see *Statistical Analysis*).

SPIKE AND PULSE-TRIGGERED AVERAGING. Time domain analysis was used to evaluate the relationship in time between the activity of elPBN or rVLM neurons and arterial BP or RSNA (18, 27, 31, 42). Neuronal activity tightly related in time to BP pulse or RSNA provides a measure of the time relationship between the neuron and cardiovascular/sympathetic activity (Figs. 3 and 6). This analysis involved arterial pulse- and renal sympathetic nerve spike-triggered averaging. A threshold was set at the systolic phase of the arterial pulse or the action potentials of the renal sympathetic nerve, while spike height discrimination and waveform recognition were used to sort action potentials of the neuron during the 300-s evaluation period. Averages of the arterial pulse or RSNA histogram and histograms of neuronal activity were constructed as demonstrated in our previous studies (18, 31, 36).

Statistical Analysis

Values are means ± SE. Effects of repeated interventions were compared using a one-way repeated-measures ANOVA with Tukey's post hoc test. If data were not normally distributed, as determined by the Kolmogorov-Smirnov test, they were compared using Friedman's repeated-measures ANOVA on ranks with Dunnett's post hoc test. Comparisons between two groups were analyzed with Student's *t*-test or the Mann-Whitney *U*-test. Statistical calculations were performed with Sigmastat software (Jandel Scientific Software, San Rafael, CA). Differences were considered statistically significant when $P < 0.05$. In addition, coherence values ≥0.5 were chosen to reflect a statistically significant relationship between neuronal activity of the elPBN or rVLM and arterial BP or RSNA (18, 31, 36, 42).

RESULTS

Activation of rVLM-Projecting elPBN Neurons in Response to CSAN Stimulation

Eleven rats in which the unilateral microinjection site of the retrograde tracer was found inside the rVLM (Fig. 1) were included in the study. The locations of injected tracer in the medulla closely matched the coordinates of the rVLM as defined by the atlas of Paxinos and Watson for the rat (37). The microinjection sites in the rat were located 12.0–12.48 mm caudal to bregma, 2.0–2.6 mm lateral from midline, and 0.2–0.7 mm from the ventral surface of the medulla. They were lateral to the paragigantocellularis nucleus, ventral to the Bötzinger complex, and medial to the VII cranial nucleus at the high rostral level (31, 37). Neurons labeled with the retrograde microsphere tracer were observed in the Kölliker-Fuse nucleus, medial PBN, and lateral PBN, including dorsal, ventral, central, and external lateral nuclei (Fig. 2). They were evaluated especially in the elPBN. We noted that approximately two-thirds of the neurons labeled with microspheres in the elPBN were located ipsilateral to the site of the unilateral injection into the rVLM. Microsphere-labeled elPBN neurons ipsilateral to the rVLM injection were counted. The number of neurons

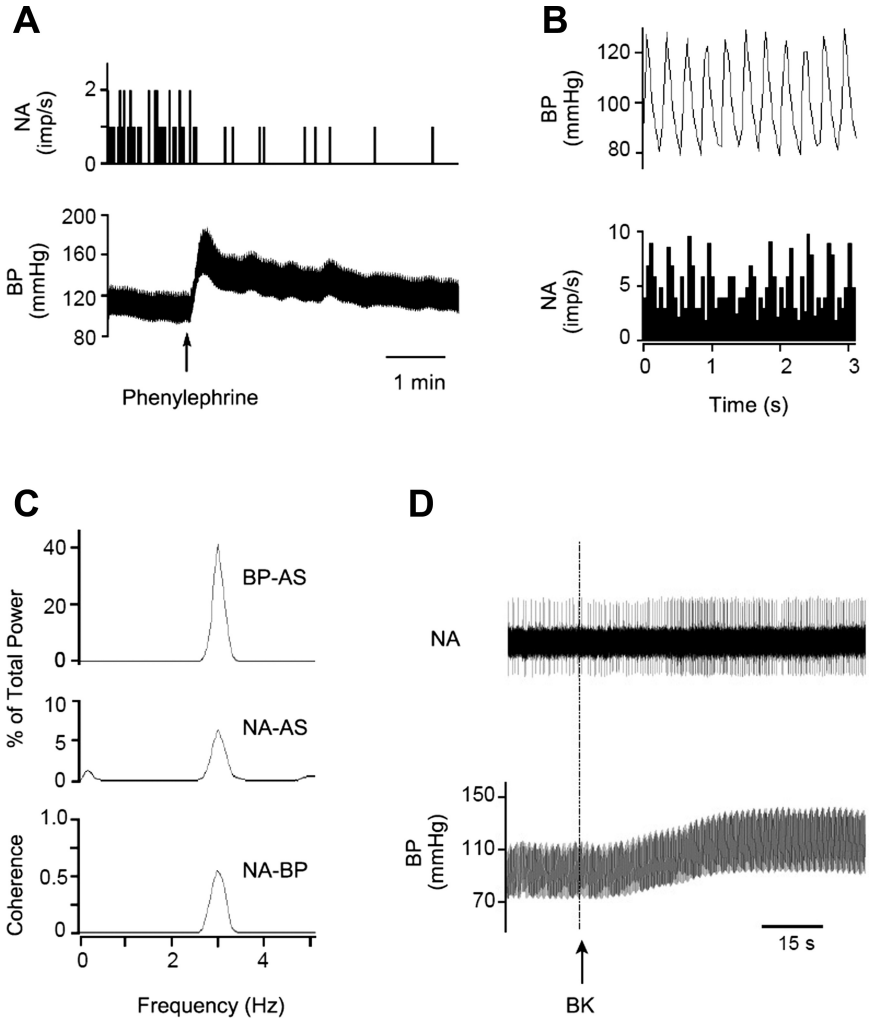

Fig. 3. Identification of a cardiovascular neuron in the elPBN. *A*: phenylephrine increased blood pressure (BP) and reduced neuronal activity (NA). *B*: time domain analysis using pulse-triggered averaging shows a relationship between BP and NA. *C*: frequency domain analysis shows a significant coherence (0.65 with frequency of 2.89 Hz) between BP and NA. *B* and *C* demonstrate cardiac rhythmicity of the elPBN neuron. *D*: NA and BP in response to stimulation of cardiac sympathetic afferent nerves with epicardial application of bradykinin (BK). *Top*: neuronal traces displaying NA; *bottom*: original recordings of BP. Arrow indicates BK application. AS, autospectra.

labeled with the retrograde microsphere tracer in the elPBN was similar in the CSAN-stimulated and control rats (Fig. 2, Table 1).

Fos-labeled neurons were noted in the Kölliker-Fuse nucleus and lateral PBN, including its ventral, central, and external lateral subdivisions, particularly in the elPBN (Figs. 1*B* and 2) The number of Fos-labeled neurons in the elPBN was increased significantly in the CSAN-stimulated group ($n = 6$) compared with the control group ($n = 5$; Table 1), consistent with our previous findings in the cat (16, 17). In the present study we found more elPBN neurons labeled with the retrograde tracer and c-Fos in the CSAN-stimulated than control rats (Fig. 2, Table 1). The proportion of elPBN double-labeled neurons projecting to the rVLM was significantly greater in the CSAN-stimulated than control group (Table 1). Figure 1, *B1–B4*, displays confocal images of neurons double-labeled with c-Fos and the retrogradely transported microspheres in the elPBN of a rat subjected to CSAN stimulation. Furthermore, neurons triple-labeled with c-Fos, the retrograde tracer, and VGLUT3, as demonstrated in Fig. 1, *C1–C4*, were frequently (6 ± 1 cells per section) identified in the elPBN of four rats following CSAN stimulation but rarely noted (1 ± 1 cells per section) in three controls. There was a significant difference in the number of triple-labeled neurons between these two groups ($P < 0.05$). The number of VGLUT3-labeled neurons in the elPBN was similar in the CSAN-stimulated and control rats.

Table 1. *c-Fos immunoreactivity and colocation with retrograde tracer in the elPBN following stimulation of CSAN*

				Tracer + Fos-Positive Cells	
	n	Fos-Positive Cells, no.	Tracer-Positive Cells, no.	Tracer + Fos-Positive Cells, no.	%Tracer-positive cells	%Fos-positive cells
Control	5	4 ± 1	28 ± 2	2 ± 1	7 ± 3	34 ± 10
CSAN stimulation	6	19 ± 3**	31 ± 4	8 ± 1**	29 ± 7*	44 ± 2

Values are means ± SE. Number of c-Fos-positive cells, neurons labeled with retrograde microsphere tracer injected into the rostral ventrolateral medulla (rVLM), and cells with both stains in the external lateral parabrachial nucleus (elPBN) are expressed per section ipsilateral to rVLM injection. Also shown is percentage of double-labeled neurons relative to number of tracer-labeled neurons or Fos-positive cells. CSAN, cardiac sympathetic afferent nerves. *$P < 0.05$, **$P < 0.01$ vs. control.

Increase in Activity of elPBN Cardiovascular Neurons by CSAN Stimulation Through Activation of Glutamate Ionotropic Receptors

In 14 cats, we found 17 elPBN neurons responsive to activation of baroreceptors. We observed that their activity was increased from 2.02 ± 0.35 to 3.14 ± 0.36 imp/s ($P < 0.05$) when MAP was lowered from 103 ± 9 to 48 ± 2 mmHg following intravenous nitroglycerin and decreased from 2.45 ± 0.33 to 1.34 ± 0.28 imp/s ($P < 0.05$) when MAP was raised from 99 ± 6 to 172 ± 5 mmHg with intravenous phenylephrine (Fig. 3*A*). Their responses to baroreceptor activation began at ~15–30 s and lasted for 90–150 s. These barosensitive cells were also tested for cardiac rhythmicity (Fig. 3, *B* and *C*) based on the time and frequency (coherence 0.7 ± 0.2 at 3 ± 0.4 Hz) domain analyses. We identified 12 cells displaying both barosensitivity and cardiac rhythmicity, i.e., cardiovascular neurons. These 12 cardiovascular neurons were responsive to both chemical (e.g., BK; Fig. 3*D*) and electrical CSAN stimulations. Their responses to epicardial application of BK started at ~8–12 s and lasted for 40–90 s. Two of the 12 elPBN cardiovascular cells responsive to CSAN stimulation were classified further as rVLM-projecting neurons, since they were activated by antidromic stimulation of the rVLM, were faithful to high-frequency rVLM stimulation, and displayed constant onset latency (Fig. 4).

We examined the activity of elPBN cardiovascular neurons in response to CSAN stimulation before and after blockade of glutamate receptors. We found that their activity in response to repeated epicardial application of BK was unchanged following iontophoresis of 0.9% normal saline into the elPBN ($n = 4$; Fig. 5*A*). However, the increased discharges induced by epicardial stimulation with BK or electrical CSAN stimulation were significantly attenuated after iontophoresis of Kyn into the elPBN ($n = 6$; Fig. 5, *B* and *D*). Basal activity of the elPBN cardiovascular neurons was not altered after administration of Kyn or 0.9% normal saline (Fig. 5).

Activation of Excitatory elPBN-rVLM Projection During CSAN Stimulation

rVLM cardiovascular neurons. We identified 25 rVLM cardiovascular neurons that were responsive to baroreceptor stimulation (Fig. 6*A*) and exhibited cardiac rhythmicity with time and frequency domain analyses (Fig. 6, *B* and *C*) in 25 cats. We observed cardiac rhythmicity with a strong correlation between rVLM activity and BP (coherence 0.85 ± 0.02). These 25 cells were responsive to both epicardial stimulation with BK and electrical CSAN stimulation. Their responses to epicardial stimulation with BK started after ~9–14 s and lasted for 40–100 s. Using spike-triggered averaging and coherence analyses, we noted a strong relationship between rVLM activity and RSNA (Fig. 6, *D* and *E*) in 18 of the 25 cardiovascular neurons (coherence 0.70 ± 0.14). These data suggest that the majority of the cardiovascular cells discharge in synchrony with the renal sympathetic nerves. They likely function as presympathetic neurons, as we and others have shown (7, 18, 22, 36). The 25 cardiovascular neurons were examined with the following protocols.

Protocol 1: rVLM neuronal response to CSAN stimulation after blockade of glutamate receptors in the elPBN. Both epicardial stimulation with BK and electrical CSAN stimulation led to consistent increases in the activity of rVLM cardiovascular neurons before and after microinjection of aCSF into the elPBN ($n = 5$; Fig. 7, *A* and *C*). In contrast, microinjection of Kyn into the elPBN significantly attenuated the increased rVLM activity induced by BK stimulation ($n = 5$; Figs. 7*B* and 8) and electrical CSAN stimulation (Fig. 7*D*). Blockade of regions surrounding the elPBN did not influence rVLM activity in response to CSAN stimulation in two cells not included

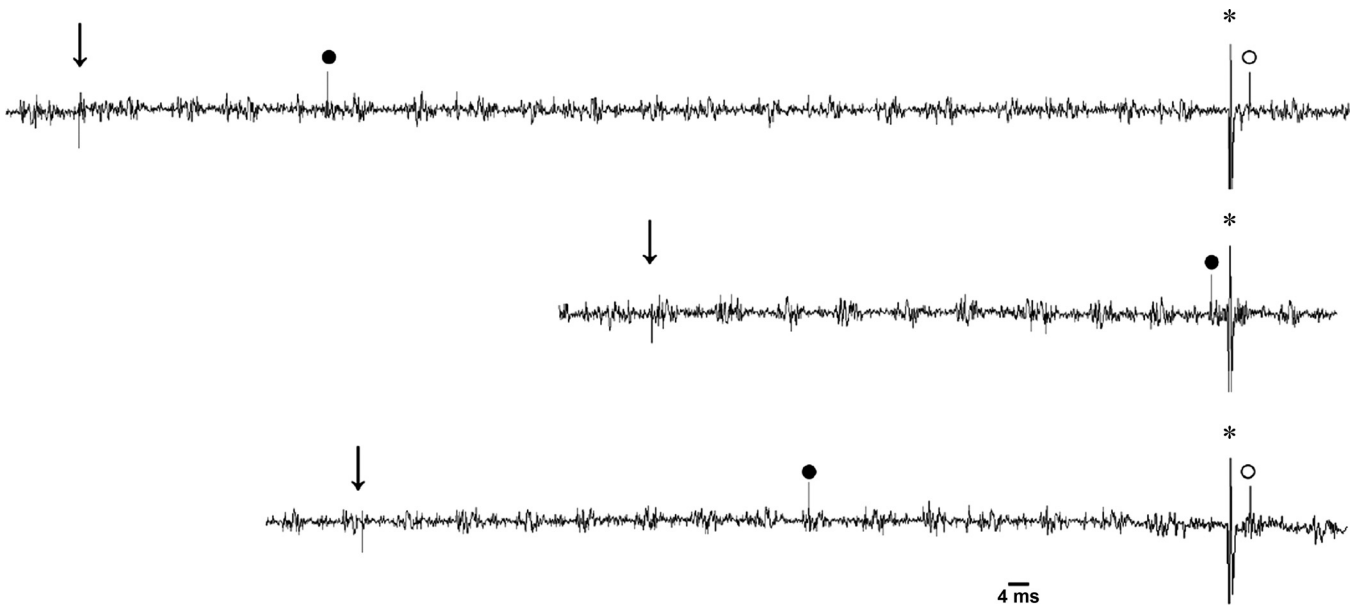

Fig. 4. Antidromic collision of an elPBN cardiovascular neuron. *Left* to *right*: time of stimulation of cardiac sympathetic afferent nerves (CSAN; ↓), CSAN-evoked elPBN spike (●), time of antidromic stimulation from rostral ventrolateral medulla (rVLM; *), and antidromic-evoked elPBN action potential (○). The neuron had a conduction velocity of 2.0 m/s, an antidromic latency of 4.0 ms, and a refractory period of 1.6 ms. *Middle trace* displays cancellation of the antidromic spike by the CSAN-evoked orthodromic spike.

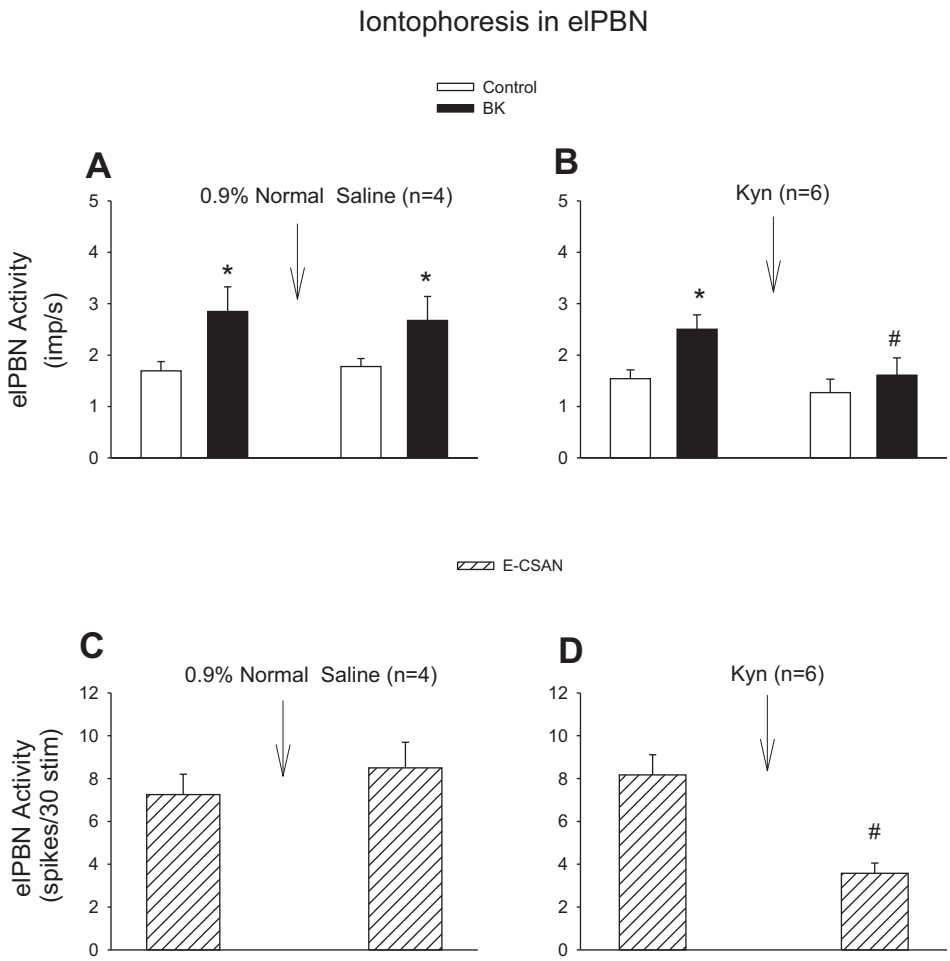

Fig. 5. Activity of elPBN cardiovascular neurons in response to stimulation of cardiac sympathetic afferent nerves (CSAN) before and after blockade of glutamate receptors. *A* and *B*: CSAN stimulation with epicardial application of bradykinin (BK, 2 μg). *C* and *D*: electrical CSAN stimulation (E-CSAN). *A* and *C*: iontophoresis of 0.9% normal saline into the elPBN. *B* and *D*: iontophoresis of kynurenic acid (Kyn, 25 mM) into the elPBN. $*P < 0.05$, after vs. before BK stimulation. $\#P < 0.05$, after vs. before iontophoresis of Kyn into the elPBN.

statistical analysis. Thus, 10 of 12 cardiovascular neurons are presented in *protocol 1*.

Protocol 2: rVLM neuronal response to elPBN excitation before and after blockade of rVLM glutamate receptors. Microinjection of aCSF, the vehicle for DLH, into the elPBN did not influence rVLM activity in the absence and presence of electrical CSAN stimulation, as described above (Fig. 7, *A* and *C*). In contrast, in 13 other rVLM cardiovascular neurons (separate from the 12 cardiovascular neurons tested in *protocol 1*), repeated microinjections of DLH (2 nmol/50 nl) into the elPBN consistently increased rVLM activity (Fig. 9). The DLH-induced increase in basal rVLM activity was not altered following iontophoresis of 0.9% normal saline into the rVLM ($n = 6$; Fig. 9*B*) but was reversed after iontophoresis of Kyn into the rVLM ($n = 7$, $P < 0.05$; Fig. 9*C*). Similarly, repeated microinjections of DLH into the elPBN consistently enhanced CSAN-evoked rVLM activity with iontophoresis of 0.9% normal saline into the rVLM (Fig. 9*D*). However, the enhanced CSAN-evoked rVLM activity by microinjection of DLH into the elPBN was significantly reduced after iontophoresis of Kyn into the rVLM (Fig. 9*E*). This reduction recovered 50–60 min later.

Anatomical Location of Recording and Stimulating Sites

Thirty-five sites of recording and microinjection (Fig. 10) were inside the elPBN, as identified by Berman's atlas for cats and consistent with our previous studies (4, 11, 16, 17). All sites in the elPBN were confined to a region 9.5–11.2 mm rostral to obex, 4.8–5.4 mm lateral to midline, and 0.7–2.1 mm from the dorsal surface of the pons, consistent with our previous study (11, 16). Two microinjections of Kyn were not located in the elPBN (Fig. 10, *B*).

All recording sites in the rVLM were confined to an area 2.8–4.2 mm rostral to obex, 2.9–3.7 mm lateral to midline, and 0.2–1.4 mm from the ventral surface, lateral to the inferior olive and pyramidal tracts, as well as ventral and medial to the facial and retrofacial nuclei (Fig. 10). These recording sites were located within the rVLM, as described by our group and others (5, 7, 18, 19, 31, 36, 42). Both the right and left sides of the elPBN and rVLM were used for microinjections and neuronal recordings in the present study. However, to more clearly show sites of microinjections and neuronal recordings, we illustrate all the sites on the left side of composite maps, since neural structures are identical in both sides of the brain region.

DISCUSSION

The present study focused on the potential role of elPBN cardiovascular neurons in regulation of rVLM neuronal activity through direct glutamatergic elPBN-rVLM pathways during cardiac sympathetic afferent stimulation. We found that cardiovascular neurons were present in the elPBN and that their

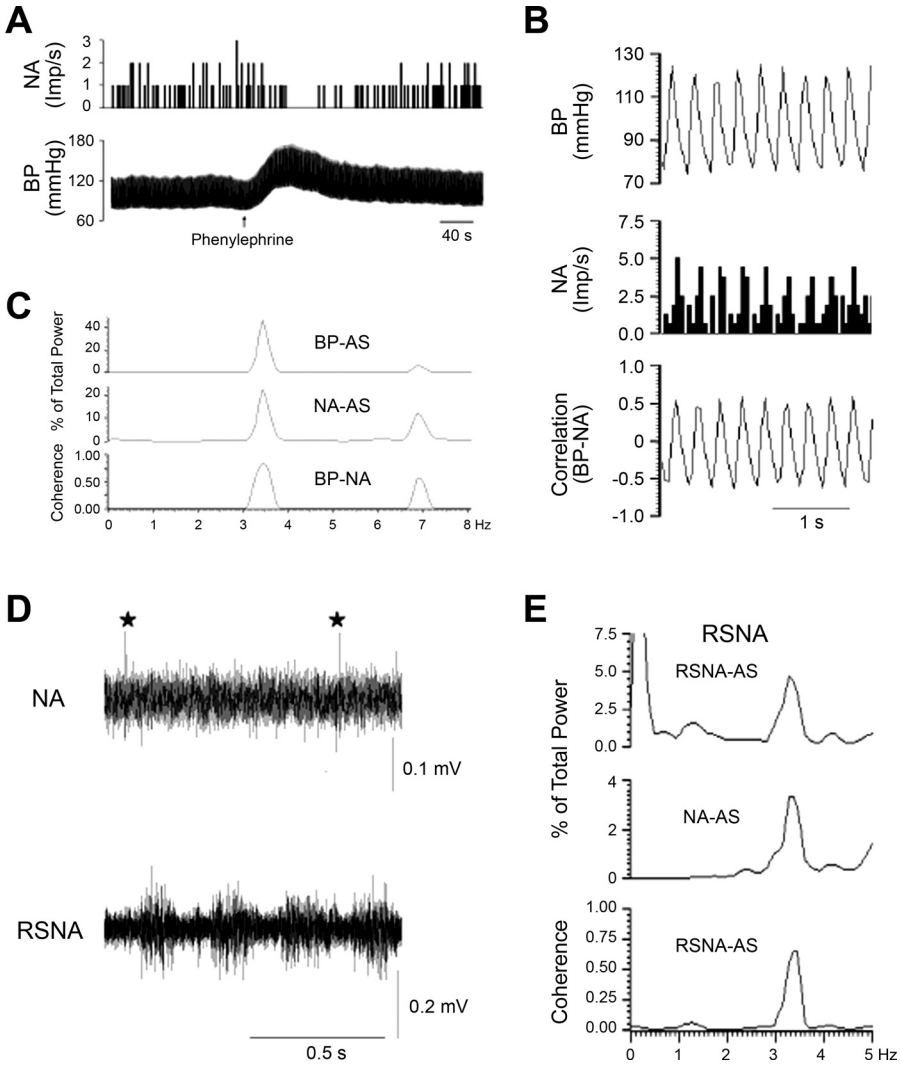

Fig. 6. Characterization of an rVLM cardiovascular neuron with sympathetic-related activity. *A*: intravenous administration of phenylephrine increased blood pressure (BP) and reduced neuronal activity (NA). *B*: pulse-triggered averaging demonstrated a correlation between BP and NA. *C*: frequency domain analysis showing a significant coherence (0.90 with frequency of 3.45 Hz) between BP and NA. *D*: NA and renal sympathetic nerve activity (RSNA). ★, Spike of the rVLM neuron. *E*: NA displayed similar rhythmicity with RSNA (coherence of 0.60 with frequency of 3.45 Hz). AS, autospectra.

activity was increased by activation of cardiac afferents following epicardial application of BK and electrical stimulation of the inferior cardiac sympathetic nerve. We also observed that blockade of glutamate receptors in the elPBN reversed the increased activity of cardiovascular neurons in the elPBN and rVLM during activation of cardiac sympathetic afferents, suggesting that elPBN cardiovascular neurons process cardiac sympathetic afferent input through glutamate to stimulate activity of rVLM cardiovascular neurons. Furthermore, using a track-tracing anatomical approach and antidromic stimulation from the rVLM, we observed that activated elPBN neurons, including cardiovascular neurons, project directly to the rVLM following cardiac sympathetic afferent stimulation. We also found that blockade of glutamate receptors in the rVLM reversed the impact of activated elPBN neurons on both basal activity of rVLM cardiovascular neurons and their increased activity during cardiac sympathetic activation. In addition, we noted that VGLUT3 was expressed in rVLM-projecting elPBN neurons activated by cardiac sympathetic afferent stimulation. These data suggest involvement of glutamate in direct projections between the elPBN and the rVLM in response to cardiac sympathetic afferent stimulation. Together, our results indicate that elPBN cardiovascular neurons, activated by cardiac sympathetic afferent stimulation, facilitate rVLM activity through direct glutamatergic projections from the elPBN to the rVLM.

Our previous study showed that the elPBN plays an important role in regulation of pressor reflexes induced by epicardial application of BK (11). Other investigators have demonstrated that the LPBN, including the elPBN, contains heterogeneous populations of neurons involved in the regulation of respiratory, cardiovascular, and gastrointestinal function (13, 23, 29). Hayward and Felder (23) reported that many neurons in the LPBN are responsive to peripheral chemoreceptor and baroreceptor inputs. They showed that most of the LPBN neurons are excited following chemoreceptor stimulation and that a majority of LPBN cells are inhibited by activation of baroreceptors (23). Unfortunately, they did not identify the cardiac rhythmicity of these PBN neurons. We and others have suggested that, in brain regions, like the rVLM and the NTS, cardiovascular neurons, by displaying both barosensitivity and cardiac rhythmicity, play a crucial role in cardiovascular regulation (1, 3, 18, 22, 36, 42). However, to our knowledge, no study has identified cardiovascular neurons in the elPBN and examined their activation by cardiac sympathetic afferent stimulation. In the present study we identified 12 cardiovascular neurons in the elPBN that were excited during epicardial stimulation with BK

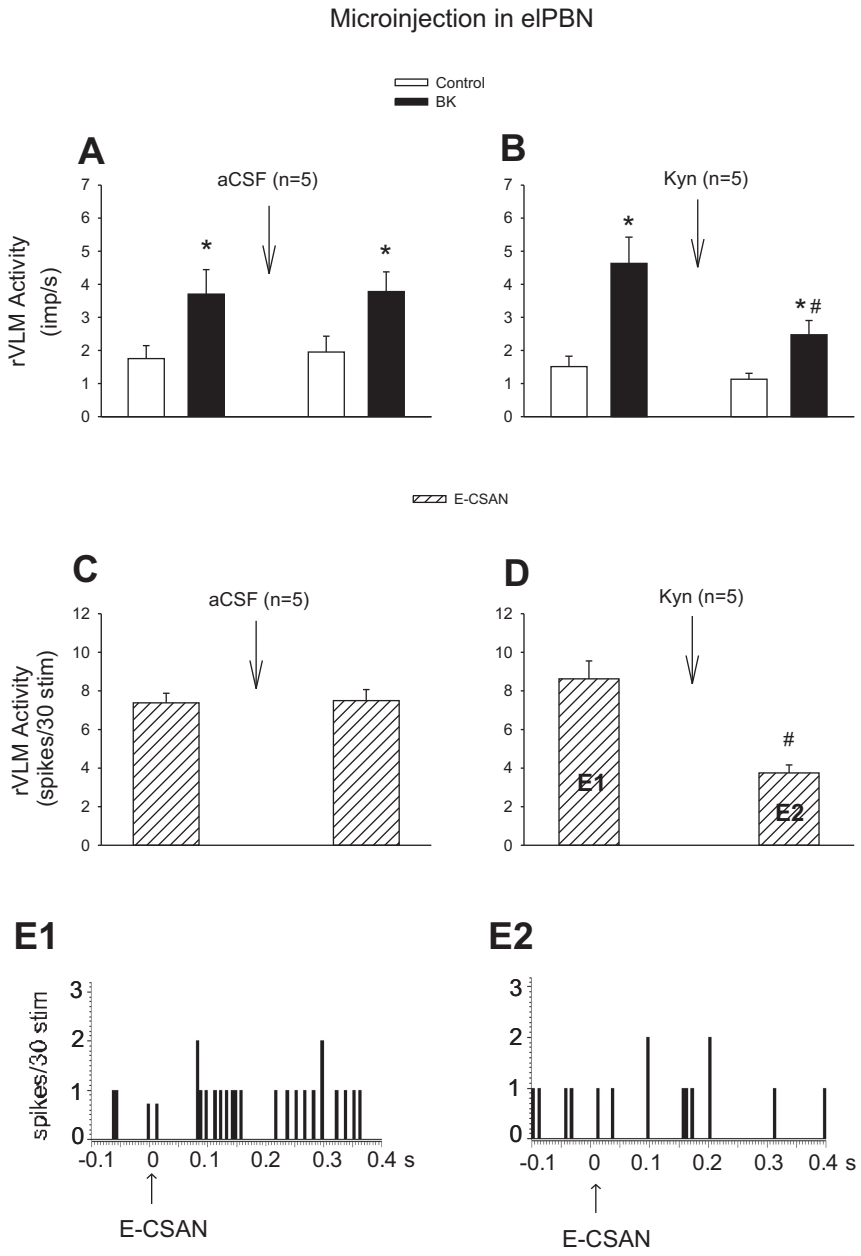

Fig. 7. Influence of blockade of glutamate receptors in the elPBN on the discharges of rVLM cardiovascular neurons in response to stimulation of cardiac sympathetic afferent nerves (CSAN). *A* and *B*: CSAN stimulation with application of bradykinin (BK, 2 μg). *C* and *D*: electrical CSAN stimulation (E-CSAN). *A* and *C*: microinjection of artificial cerebrospinal fluid (aCSF) into the elPBN. *B* and *D*: microinjection of kynurenic acid (Kyn, 25 mM) into the elPBN. $*P < 0.05$, after vs. before BK stimulation. $\#P < 0.05$, after vs. before microinjection of Kyn into the elPBN. *E1* and *E2* in hatched-bar histograms in *D* represent peristimulus histograms of an individual neuron shown in *E1* and *E2*. Arrows in *E1* and *E2* indicate electrical CSAN stimulation.

and electrical cardiac sympathetic afferent stimulation. Furthermore, we observed that the increased activity of these elPBN neurons is suppressed following blockade of glutamate receptors in the elPBN. These new findings are congruent with our previous data on sympathoexcitatory pressor responses induced by epicardial stimulation with BK (11), indicating that cardiovascular neurons in the elPBN are excited by glutamate during cardiac sympathetic afferent activation.

Anatomical and functional evidence has shown connections between the elPBN and the rVLM in rats and cats (7, 13, 30a, 35, 39). An anterograde autoradiographic study showed connections between the LPBN and the rVLM in rats (39). In cats, Miura and Takayama (35) reported that microinjection of glutamate into the LPBN induces a pressor-depressor response through LPBN-rVLM projections. Although with c-Fos we previously observed that cardiac sympathetic afferent stimulation activated elPBN neurons in cats (17), it was unclear whether these activated elPBN neurons project directly to the rVLM. The present study used a double-labeling approach in rats to verify direct projections from cardiac sympathetic-activated elPBN cells to the rVLM. Similarly, antidromic stimulation of the rVLM activated elPBN cardiovascular neurons in cats. Since numerous studies indicate that the anatomical circuitry in the cardiovascular responses in rats and cats is virtually identical (6, 7, 21, 25, 42, 49), we believe that the physiological and anatomical data obtained in the current study in the two species are mutually supportive.

We observed previously in cats that cardiac sympathetic-activated elPBN neurons contain VGLUT3 (17). VGLUT3 transports glutamate into neuronal vesicles and, thus, is considered by many to be a useful marker to identify neurons that use glutamate as a neurotransmitter (9, 15, 17, 32). The present

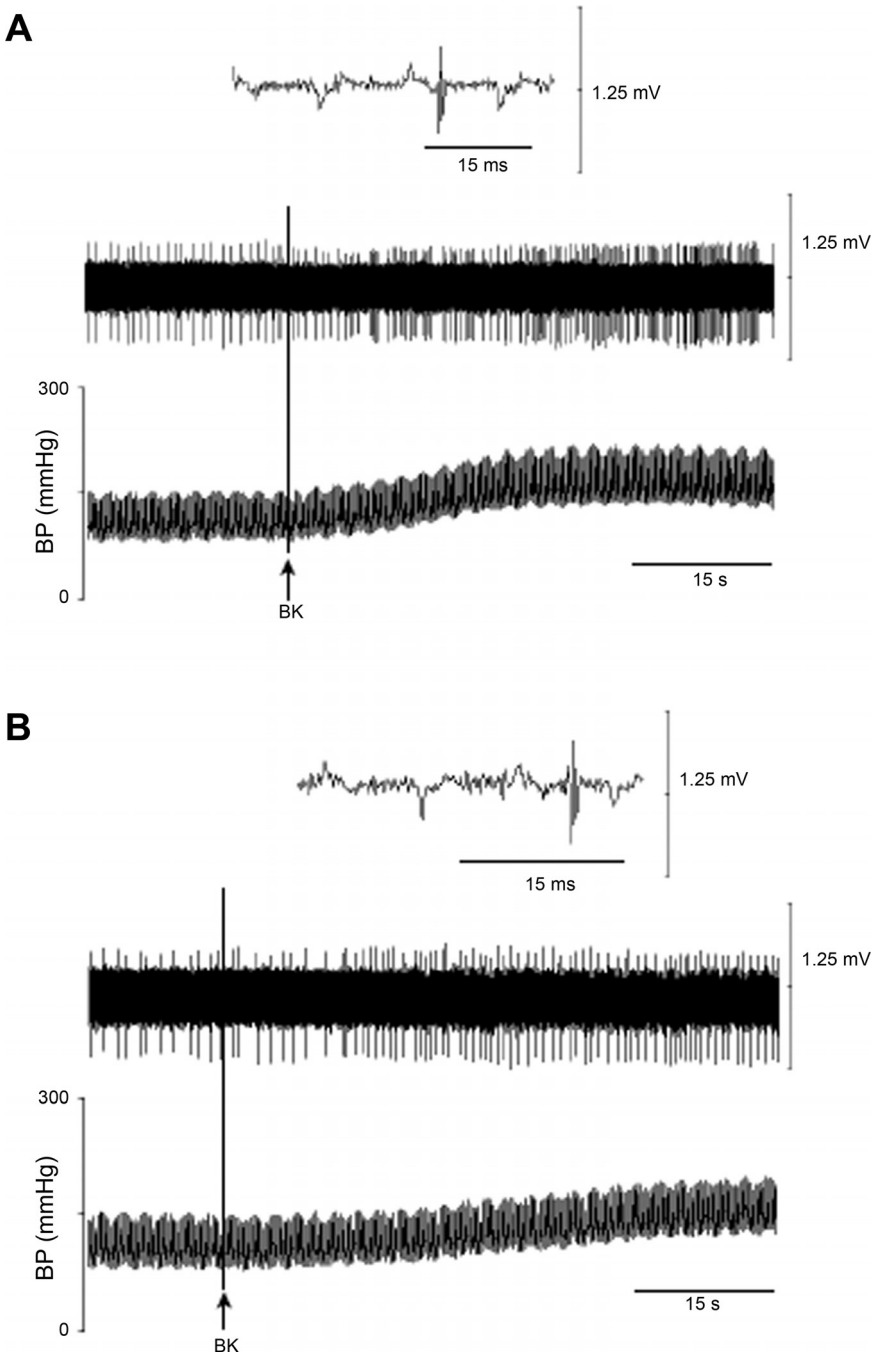

Fig. 8. Activity of an rVLM cardiovascular neuron in response to epicardial application of bradykinin (BK, 2 μg) before (*A*) and 5 min after (*B*) unilateral microinjection of kynurenic acid (Kyn, 25 mM) into the elPBN in 1 cat. *A* and *B*: an rVLM action potential (*top*), neuronal traces displaying rVLM activity (*middle*), and original arterial blood pressure (BP) recordings (*bottom*). Arrows indicate BK application.

anatomical data documented VGLUT3 expression in rVLM-projecting elPBN neurons, suggesting its potential influence. Furthermore, the present electrophysiological results demonstrate that blockade of glutamate inotropic receptors in the rVLM reverses both the enhanced basal and cardiac sympathetic afferent-evoked rVLM discharge induced during excitation of the elPBN with DLH. Together, these results suggest that elPBN glutamatergic neurons projecting directly to the rVLM are involved in central neural processing during cardiac sympathetic nerve stimulation.

In the present studies, using frequency and time domain analyses, we identified cardiovascular neurons in the elPBN and rVLM on the basis of their responses to activation/inhibition of baroreceptors and their relationships to cardiac rhythmicity, as documented by our group and others (14, 18, 22, 27, 36, 42, 43). Moreover, sympathetic-related activity is observed in the majority (72%) of the rVLM cells. As such, rVLM cardiovascular neurons tested in the present study likely function as sympathoexcitatory neurons, as we and others have shown previously (7, 18, 22, 36). However, previous studies have not examined the influence of elPBN cardiovascular neurons on the rVLM sympathoexcitatory neuronal activity during activation of CSAN. The present study demonstrates that blockade of glutamate receptors in the elPBN attenuates the increased activity of the rVLM cardiovascular neurons during CSAN stimulation, while excitation of cell bodies, but

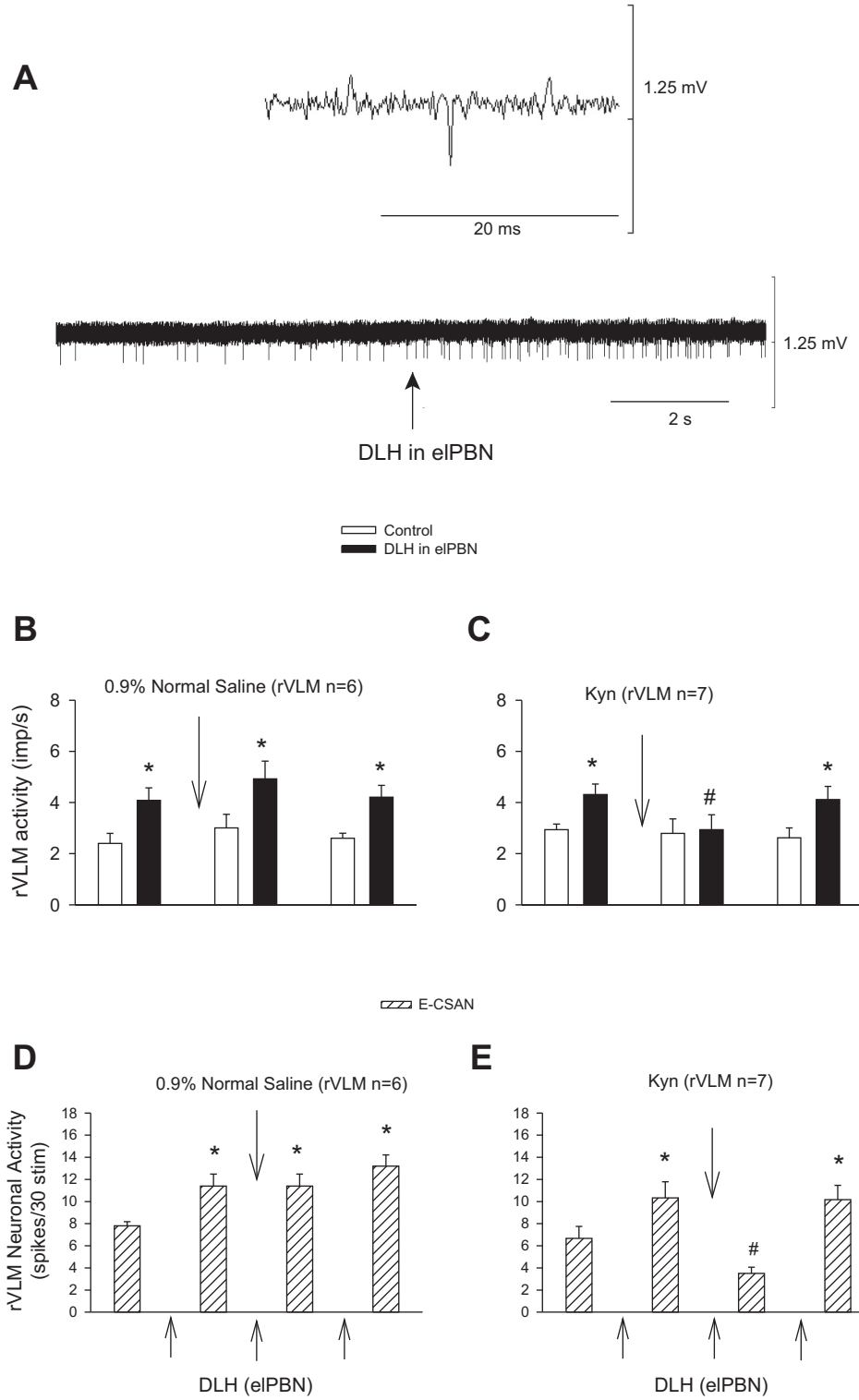

Fig. 9. Activation of the elPBN through glutamate regulates rVLM activity in the absence and presence of CSAN stimulation. *A*: neuronal traces of an rVLM cardiovascular neuron in response to microinjection of DL-homocysteic acid (DLH, 2 nmol/50 nl) into the elPBN. An individual action potential is shown above traces. *B* and *C*: increased basal rVLM activity in response to microinjection of DLH into the elPBN. *D* and *E*: evoked rVLM activity induced by electrical CSAN stimulation (E-CSAN) in response to microinjection of DLH into the elPBN. DLH-enhanced basal and CSAN-evoked activity in the rVLM recovered 50–60 min after Kyn. $*P < 0.05$, after vs. before elPBN excitation with DLH. $\#P < 0.05$, after vs. before iontophoresis of Kyn into the rVLM.

not fibers of passage in the elPBN with DLH (1, 7), increases the basal and CSAN-evoked activity of the rVLM cardiovascular neurons. These physiological data indicate that elPBN cardiovascular neurons participate in central regulation of rVLM neuronal activity through elPBN-rVLM projections during cardiac sympathetic afferent stimulation.

There are two potential limitations in the present study. First, although we were able to record the activity of elPBN neurons in response to antidromic stimulation in the rVLM, it was not feasible technically to stimulate and record the same neuron simultaneously. Thus we were unable to test responsiveness of both elPBN and rVLM neurons following cardiac sympathetic afferent stimulation and to examine if blocking elPBN neurons attenuates increased rVLM activity during cardiac sympathetic afferent stimulation in a single antidromic experiment. However, we have shown that inhibition of elPBN neurons (possi-

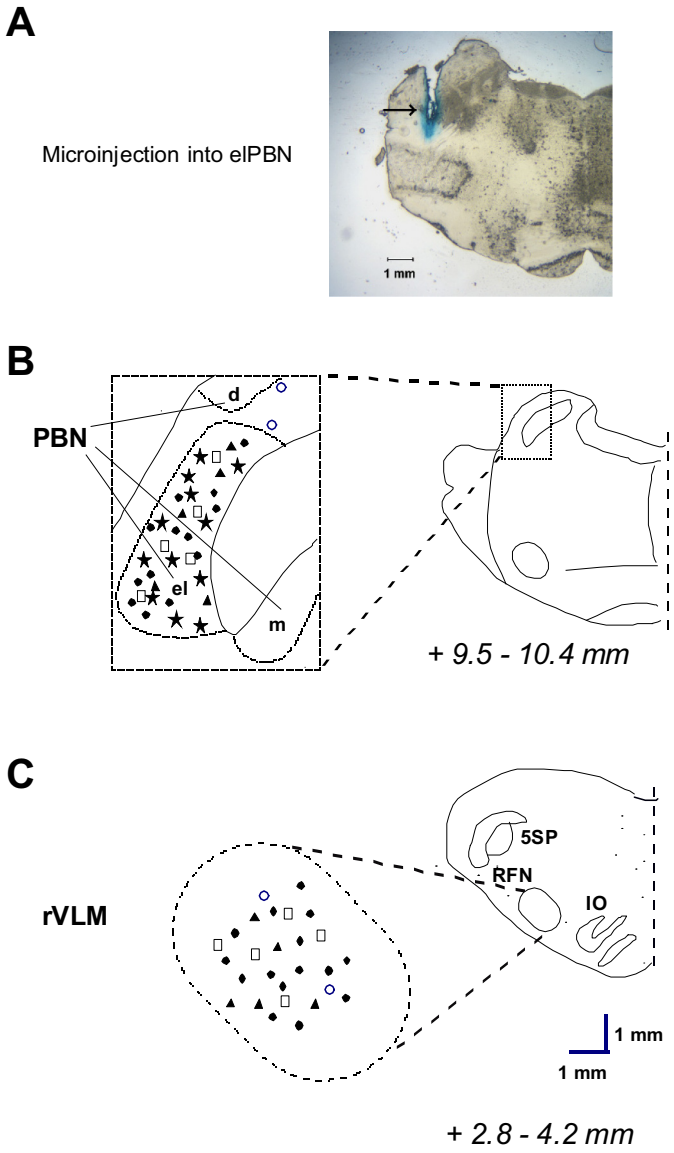

Fig. 10. Anatomical locations of microinjection and neuronal recording sites. *A*: an original slide of the pons (+9.8 mm from obex) showing an actual microinjection site (arrow) in the elPBN of a cat. *B* and *C*: composite maps displaying histologically verified sites of microinjections and neuronal recordings in the elPBN (*B*) and rVLM (*C*) in cats. *Left*: magnified areas indicated by boxes at *right*. Brain sections indicate combinations of planes of brain stem rostral to the obex (Berman's atlas for the cat). ★, Recording in the elPBN; □, ▲, and ●, microinjection of aCSF, kynurenic acid, or DL-homocysteic acid, respectively, into the elPBN and recording in the rVLM in the cat; ○, microinjection of kynurenic acid outside the elPBN and recording in the rVLM in the cat. BC, brachium conjunctivum; PBN, parabrachial nucleus; dPBN, dorsal lateral subnucleus of PBN; elPBN, external lateral PBN; mPBN, medial subnucleus of PBN; ION, inferior olivary nucleus; RFN, retrofacial nucleus.

bly including rVLM-projecting neurons) attenuate increased rVLM activity induced by cardiac sympathetic afferent activation. Thus the present anatomical and physiological findings, in combination, suggest that elPBN cardiovascular neurons projecting to the rVLM likely influence rVLM activity during cardiac sympathetic afferent activation.

Second, in the present immunohistochemical experiments, we employed VGLUT3 as a marker of potential glutamatergic pathways in the elPBN-rVLM projections during cardiac sympathetic activation. There is a possibility that GABAergic and/or cholinergic pathways play a role in the elPBN-rVLM projection, since previous studies reported that VGLUT3 also is expressed in GABAergic and cholinergic neurons (9, 15, 17). However, the present electrophysiological data show that blockade of glutamate receptors in the rVLM reverses the impact of activated elPBN neurons on rVLM activity, supporting the conclusion that glutamatergic synaptic transmission is required for elPBN-induced stimulation of rVLM neurons. Furthermore, Gritti et al. (15) showed that the majority (96–100%) of VGLUT3-labeled neurons stain positively for phosphate-activated glutaminase, an enzyme that synthesizes glutamate from glutamine and is enriched in glutamatergic neurons. Therefore, it is likely that during cardiac sympathetic activation glutamate mediates the action of the elPBN on rVLM neurons.

Perspectives and Significance

In summary, the present study indicates that elPBN cardiovascular neurons regulate rVLM activity through excitatory elPBN-rVLM projections during cardiac sympathetic afferent stimulation, suggesting that elPBN and elPBN-rVLM neural pathways are important in regulation of cardiac sympathoexcitatory reflex responses. These results extend our understanding of the importance of elPBN cardiovascular neurons and direct glutamatergic elPBN-rVLM neural pathways in central-processing sympathoexcitatory reflex responses induced by cardiac sympathetic afferent stimulation.

The elPBN is also connected to several other nuclei, including the hypothalamic paraventricular nucleus and the NTS (7, 13). We have demonstrated that these nuclei also are activated by cardiac sympathetic afferent stimulation (19, 20), implying that additional pathways may be involved in central regulation of rVLM activity and in processing of cardiac-cardiovascular reflex responses. In this regard, projections among the elPBN-hypothalamic paraventricular nucleus and/or the elPBN-NTS may participate in the central regulation of rVLM activity and cardiac sympathoexcitatory reflex responses during activation of CSAN (7, 13, 39). No other study has examined the contribution of the above-mentioned pathways in these processes during cardiac sympathetic afferent stimulation. Future investigations are needed to determine the contributions of the aforementioned pathways in central regulation of rVLM activity and sympathoexcitatory reflexes in response to activation of cardiac afferents, in particular during myocardial ischemia.

ACKNOWLEDGMENTS

The authors gratefully acknowledge the technical assistance of Jesse Ho.

GRANTS

This work was supported by National Heart, Lung, and Blood Institute Grants HL-66217 (L.-W. Fu and J. C. Longhurst) and HL-72125 (S. C. Tjen-A-Looi and J. C. Longhurst). J. C. Longhurst held the Larry K. Dodge and Susan Samueli Endowed Chairs. Z.-L. Guo was the recipient of the Department of Medicine Chair's Research Award, University of California at Irvine.

DISCLOSURES

No conflicts of interest, financial or otherwise, are declared by the authors.

AUTHOR CONTRIBUTIONS

Z.L.G, J.C.L, S.C.T.-A-L, and L.-W.F. developed the concept and designed the research; Z.-L.G., S.C.T.-A-L., and L.-W.F. performed the experiments;

Z.-L.G., S.C.T.-A-L. and L.-W.F. analyzed the data; Z.-L.G., S.C.T.-A-L. and L.-W.F. interpreted the results of the experiments; Z.-L.G., S.C.T.-A-L., and L.-W.F. prepared the figures; Z.-L.G, J.C.L, S.C.T.-A-L, and L.-W.F. drafted the manuscript; Z.-L.G., J.C.L., S.C.T.-A-L., and L.-W.F. edited and revised the manuscript; Z.-L.G, J.C.L, S.C.T.-A-L, and L.-W.F. approved the final version of the manuscript.

REFERENCES

1. **Agarwal SK, Calaresu FR.** Supramedullary inputs to cardiovascular neurons of rostral ventrolateral medulla in rats. *Am J Physiol Regul Integr Comp Physiol* 265: R111–R116, 1993.
2. **Agarwal SK, Gelsema AJ, Calaresu FR.** Inhibition of rostral VLM by baroreceptor activation is relayed through caudal VLM. *Am J Physiol Regul Integr Comp Physiol* 258: R1271–R1278, 1990.
3. **Balan JA, Caous CA, Yu YG, Lindsey CJ.** Barosensitive neurons in the rat tractus solitarius and paratrigeminal nucleus: a new model for medullary, cardiovascular reflex regulation. *Can J Physiol Pharmacol* 82: 474–484, 2004.
4. **Berman AL.** *The Brainstem of the Cat: A Cytoarchitectonic Atlas With Stereotaxic Coordinates*. Madison: University of Wisconsin Press, 1968.
5. **Campos RR, McAllen RM.** Cardiac sympathetic premotor neurons. *Am J Physiol Regul Integr Comp Physiol* 272: R615–R620, 1997.
6. **Chamberlin N, Saper C.** Topographic organization of cardiovascular responses to electrical and glutamate microstimulation of the parabrachial nucleus in the rat. *J Comp Neurol* 326: 245–262, 1992.
7. **Dampney RA.** Functional organization of central pathways regulating the cardiovascular system. *Physiol Rev* 74: 323–364, 1994.
8. **Degtyarenko AM, Kaufman MP.** Barosensory cells in the nucleus tractus solitarius receive convergent input from group III muscle afferents and central command. *Neuroscience* 140: 1041–1050, 2006.
9. **Fremeau RJ, Burman J, Qureshi T, Tran C, Proctor J, Johnson J, Zhang H, Sulzer D, Copenhagen D, Storm-Mathisen J, Reimer R, Chaudry F, Edwards R.** The identification of vesicular glutamate transporter 3 suggests novel modes of signaling by glutamate. *Proc Natl Acad Sci USA* 99: 14488–14493, 2002.
10. **Fu LW, Barvarz S, Ho J, Longhurst JC.** Opioid receptors modulate the excitatory cardiovascular reflex responses to myocardial ATP stimulation through a P2 receptor mechanism (Abstract). *FASEB J* 26: 1091–4, 2012.
11. **Fu LW, Guo ZL, Longhurst JC.** Ionotropic glutamate receptors in the external lateral parabrachial nucleus participate in processing cardiac sympathoexcitatory reflexes. *Am J Physiol Heart Circ Physiol* 302: H1444–H1453, 2012.
12. **Fu LW, Longhurst JC.** A new function for ATP: activating cardiac sympathetic afferents during myocardial ischemia. *Am J Physiol Heart Circ Physiol* 299: H1762–H1771, 2010.
13. **Fulwiler C, Saper C.** Subnuclear organization of the efferent connections of the parabrachial nucleus in the rat. *Brain Res* 319: 229–259, 1984.
14. **Gebber GL, Barman SM, Kocsis B.** Coherence of medullary unit activity and sympathetic nerve discharge. *Am J Physiol Regul Integr Comp Physiol* 259: R561–R571, 1990.
15. **Gritti I, Henny P, Galloni F, Mainville L, Mariotti M, Jones BE.** Stereological estimates of the basal forebrain cell population in the rat, including neurons containing choline acetyltransferase, glutamic acid decarboxylase or phosphate-activated glutaminase and colocalizing vesicular glutamate transporters. *Neuroscience* 143: 1051–1064, 2006.
16. **Guo ZL, Li P, Longhurst J.** Central pathways in the pons and midbrain involved in cardiac sympathoexcitatory reflexes in cats. *Neuroscience* 113: 433–444, 2002.
17. **Guo ZL, Moazzami A, Longhurst J.** Stimulation of cardiac sympathetic afferent activates glutamatergic neurons in the parabrachial nucleus: relation to neurons containing nNOS. *Brain Res* 1053: 97–107, 2005.
18. **Guo ZL, Tjen-A-Looi SC, Fu LW, Longhurst JC.** Nitric oxide in rostral ventrolateral medulla regulates cardiac-sympathetic reflex: role of synthase isoforms. *Am J Physiol Heart Circ Physiol* 297: H1479–H1486, 2009.
19. **Guo Z, Lai H, Longhurst J.** Medullary pathways involved in cardiac sympathoexcitatory reflexes in the cat. *Brain Res* 925: 55–66, 2002.
20. **Guo Z, Moazzami A.** Involvement of nuclei in the hypothalamus in cardiac sympathoexcitatory reflexes in cats. *Brain Res* 1006: 36–48, 2004.
21. **Hade JS, Mifflin SW, Donta TS, Felder RB.** Stimulation of parabrachial neurons elicits a sympathetically mediated pressor response in cats. *Am J Physiol Heart Circ Physiol* 255: H1349–H1358, 1988.
22. **Hayes K, Calaresu FR, Weaver LC.** Pontine reticular neurons provide tonic excitation to neurons in rostral ventrolateral medulla in rats. *Am J Physiol Regul Integr Comp Physiol* 266: R237–R244, 1994.
23. **Hayward LF, Felder RB.** Peripheral chemoreceptor inputs to the parabrachial nucleus of the rat. *Am J Physiol Regul Integr Comp Physiol* 268: R707–R714, 1995.
24. **Huang HS, Stahl G, Longhurst J.** Cardiac-cardiovascular reflexes induced by hydrogen peroxide in cats. *Am J Physiol Heart Circ Physiol* 268: H2114–H2124, 1995.
25. **Kantzides A, Badoer E.** Activation of NADPH-diaphorase-positive projections to the rostral ventrolateral medulla following cardiac mechanoreceptor stimulation in the conscious rat. *Am J Physiol Regul Integr Comp Physiol* 290: R1626–R1638, 2006.
26. **Katz LC, Burkhalter A, Dreyer WJ.** Fluorescent latex microspheres as a retrograde neuronal marker for in vivo and in vitro studies of visual cortex. *Nature* 310: 498–500, 1984.
27. **Kocsis B, Gebber GL, Barman SM, Kenney MJ.** Relationships between activity of sympathetic nerve pairs: phase and coherence. *Am J Physiol Regul Integr Comp Physiol* 259: R549–R560, 1990.
28. **Kubo T, Hagiwara Y, Sekiya D, Fukumori R.** Evidence for involvement of the lateral parabrachial nucleus in mediation of cholinergic inputs to neurons in the rostral ventrolateral medulla of the rat. *Brain Res* 789: 23–31, 1998.
29. **Lara JP, Parkes MJ, Silva-Carvhalo L, Izzo P, wid-Milner MS, Spyer KM.** Cardiovascular and respiratory effects of stimulation of cell bodies of the parabrachial nuclei in the anaesthetized rat. *J Physiol* 477: 321–329, 1994.
30. **Lawrence AJ, Jarrott B.** Neurochemical modulation of cardiovascular control in the nucleus tractus solitarius. *Prog Neurobiol* 48: 21–53, 1996.

30a. **Len WB, Chan Y.** Glutamatergic projection to RVLM mediates suppression of reflex bradycardia by parabrachial nucleus. *Am J Physiol Heart Circ Physiol* 276: H1482–H1492, 1999.

31. **Li P, Tjen-A-Looi SC, Guo ZL, Fu LW, Longhurst JC.** Long-loop pathways in cardiovascular electroacupuncture responses. *J Appl Physiol* 106: 620–630, 2009.
32. **Lin LH, Talman WT.** Nitroxidergic neurons in rat nucleus tractus solitarii express vesicular glutamate transporter 3. *J Chem Neuroanat* 29: 179–191, 2005.
33. **Lipski J.** Antidromic activation of neurones as an analytic tool in the study of the central nervous system. *J Neurosci Methods* 4: 1–32, 1981.
34. **Meller ST, Gebhart GF.** A critical review of the afferent pathways and the potential chemical mediators involved in cardiac pain. *Neuroscience* 48: 501–524, 1992.
35. **Miura M, Takayama K.** Circulatory and respiratory responses to glutamate stimulation of the lateral parabrachial nucleus of the cat. *J Auton Nerv Syst* 32: 121–133, 1991.
36. **Moazzami A, Tjen-A-Looi SC, Guo ZL, Longhurst JC.** Serotonergic projection from nucleus raphe pallidus to rostral ventrolateral medulla modulates cardiovascular reflex responses during acupuncture. *J Appl Physiol* 108: 1336–1346, 2010.
37. **Paxinos G, Watson C.** *The Rat Brain in Stereotaxic Coordinates*. New York: Academic, 2009.
38. **Salo LM, Nalivaiko E, Anderson CR, McAllen RM.** Control of cardiac rate, contractility, and atrioventricular conduction by medullary raphe neurons in anesthetized rats. *Am J Physiol Heart Circ Physiol* 296: H318–H324, 2009.
39. **Saper CB, Loewy AD.** Efferent connections of the parabrachial nucleus in the rat. *Brain Res* 197: 291–317, 1980.
40. **Shin K, Minamitani H, Onishi S, Yamazaki H, Lee M.** Assessment of training-induced autonomic adaptations in athletes with spectral analysis of cardiovascular variability signals. *Jpn J Physiol* 45: 1053–1069, 1995.
41. **Tjen-A-Looi SC, Bonham A, Longhurst JC.** Interactions between sympathetic and vagal cardiac afferents in nucleus tractus solitarii. *Am J Physiol Heart Circ Physiol* 272: H2843–H2851, 1997.
42. **Tjen-A-Looi SC, Li P, Longhurst JC.** Role of medullary GABA, opioids, and nociceptin in prolonged inhibition of cardiovascular sympathoexcitatory reflexes during electroacupuncture in cats. *Am J Physiol Heart Circ Physiol* 293: H3627–H3635, 2007.
43. **Tseng WT, Chen RF, Tsai ML, Yen CT.** Correlation of discharges of rostral ventrolateral medullary neurons with the low-frequency sympathetic rhythm in rats. *Neurosci Lett* 454: 22–27, 2009.
44. **Turner A, Kumar N, Farnham M, Lung M, Pilowsky P, McMullan S.** Rostroventrolateral medulla neurons with commissural projections pro-

vide input to sympathetic premotor neurons: anatomical and functional evidence. *Eur J Neurosci* 38: 2504–2515, 2013.
45. **Urbanksi RW, Sapru HN.** Putative neurotransmitters involved in medullary cardiovascular regulation. *J Auton Nerv Syst* 25: 181–193, 1988.
46. **Vercelli A, Repici M, Garbossa D, Grimaldi A.** Recent techniques for tracing pathways in the central nervous system of developing and adult mammals. *Brain Res Bull* 51: 11–28, 2000.
47. **Wang H, Weston MC, McQuiston TJ, Stornetta RL, Guyenet PG.** Neurokinin-1 receptor-expressing cells regulate depressor region of rat ventrolateral medulla. *Am J Physiol Heart Circ Physiol* 285: H2757–H2769, 2003.
48. **Zhao XL, Yan JQ, Yang XJ, Chen K, Li JR, Zhang Y.** Fos positive neurons in the brain stem and amygdala mostly express vesicular glutamate transporter 3 after bitter taste stimulation. *Brain Res* 1445: 20–29, 2012.
49. **Zhou W, Tjen-A-Looi S, Longhurst JC.** Brain stem mechanisms underlying acupuncture modality-related modulation of cardiovascular responses in rats. *J Appl Physiol* 99: 851–860, 2005.